# Dominant negative mutations in yeast Hsp90 reveal triage decision mechanism targeting client proteins for degradation

Julia M. Flynn, Margot E. Joyce, Daniel N. A. Bolon[#]

Department of Biochemistry and Molecular Biotechnology
University of Massachusetts Chan Medical School
Worcester, MA 01605 USA

[#]Dan.Bolon@umassmed.edu

Abstract

Most of the fundamental processes of cells are mediated by proteins. However, the biologically-relevant mechanism of most proteins are poorly understood. Dominant negative mutations have provided a valuable tool for investigating mechanism, but can be difficult to isolate because of their toxic effects. We used a mutational scanning approach to identify dominant negative mutations in yeast Hsp90. Hsp90 is a chaperone that forms dynamic complexes with many co-chaperones and client proteins. In vitro analyses have elucidated some key biochemical states and structures of Hsp90, co-chaperones, and clients; however, the biological mechanism of Hsp90 remains unclear. For example, high throughput studies have found that many E3 ubiquitin ligases bind to Hsp90, but it is unclear if these are primarily clients or acting to tag other clients for degradation. Our analysis of all point mutations in Hsp90 identified 205 that dramatically slowed the growth of yeast harboring a second WT copy of Hsp90. 75% of the dominant negative mutations that we identified were located in a loop that closes over bound ATP. We analyzed a small panel of individual dominant mutations in this loop in detail. In this panel, addition of the E33A mutation that prevents ATP hydrolysis by Hsp90 abrogated the dominant negative phenotype. Pull-down experiments did not reveal any stable binding partners, indicating that the dominant effects were mediated by dynamic complexes. We examined the stability to proteolysis of glucocorticoid receptor (GR) as a model Hsp90 substrate. Upon expression of dominant negative Hsp90 variants, GR was rapidly destabilized in a proteasome-dependent fashion. These findings provide evidence that the binding of E3 ligases to Hsp90 may serve a quality control function fundamental to eukaryotes.

## Introduction

Understanding protein mechanism is fundamental to understanding life because proteins carry out most of the biochemical reactions in living organisms. Where protein mechanisms have been successfully revealed, they have led to key biological insights [1,2] and valuable biotechnology [3]. While science has made tremendous strides in illuminating ground state structures of many proteins, protein function often relies on transiently populated states (e.g. transition states in enzymes or dynamic binding interactions) that remain challenging to investigate. Investigating the mechanism of proteins that function as interaction hubs is made more difficult because of the importance of studying function with all relevant binding partners present.

Dominant negative mutations that impede function in the presence of a wildtype (WT) copy provide a powerful approach to identify key mechanistic steps [4,5]. Dominant negative mutations have a rich history in the study of protein mechanism, though they have not been utilized widely in part because they tend to be toxic making them difficult to identify by traditional genetic screens. We recently developed mutational scanning approaches to identify dominant negative mutations in yeast [6,7]. In these studies, systematic libraries of all possible point mutations in a gene were expressed and toxic variants that slowed growth in a bulk competition were identified based on decreased frequency using a deep sequencing readout. Here, we used mutational scanning to study dominant negative mutations in the Hsp90 molecular chaperone.

Hsp90 is an essential chaperone in eukaryotes [8] where it is required for the maturation of client proteins to mature and active conformations [9]. While many chaperones including Hsp40 and Hsp70 that bind to unfolded or misfolded conformations, Hsp90 binds to many clients in folded conformations that closely resemble their structure in the absence of chaperone [9]. High-throughput studies indicate that more than half of human kinases bind to Hsp90 [10]. High-throughput analyses also show that about 30% of mammalian E3 ligases bind to Hsp90 [10], though it is not clear how many of these are clients of Hsp90 and/or act to stimulate degradation of Hsp90 clients. Hsp90 also assists in ligand binding to many nuclear steroid hormone receptors [11]. For example, studies of glucocorticoid receptor (GR) show that the steroid binding site is located in the interior of the protein structure and inaccessible to ligand binding in the absence of Hsp90 [12,13].

Small molecule inhibitors of Hsp90 have shown promise as anti-cancer agents [14]. Early studies demonstrated that geldanamycin, a natural product known to revert the transforming phenotype of v-src in mammalian cells in culture acted indirectly by inhibiting Hsp90 rather than v-src [15]. Potent synthetic inhibitors of Hsp90 have been developed and investigated as anti-cancer therapeutics [16]. While Hsp90 inhibitors have not yet been approved for therapeutic use, they have revealed important insights into Hsp90 mechanism. For example, Hsp90 inhibitors stimulate the ubiquitin-dependent degradation of many Hsp90 client proteins [17]. The association of many human E3 ubiquitin ligases with Hsp90 [10] suggests that some of these E3 enzymes function with Hsp90 in triage decisions where clients that cannot be matured to active conformations are instead targeted for degradation. Strong evidence shows that the human E3 CHIP serves this triage function with Hsp90. CHIP contains a TPR domain that binds in its native state to the C-

terminus of Hsp90 leaving its ubiquitin ligase domain proximity to clients [18–20]. While the triage role of CHIP is known, the potential role of other E3's in triage decisions is unclear. Of note, there is no clear homologue of the CHIP E3 ligase in yeast, and it is unknown if the triage function of Hsp90 is conserved across eukaryotes. It is also unclear how Hsp90 functions with CHIP or other E3's to make triage decisions. For example, what are the molecular signatures that determine if a client will be chaperoned or targeted for destruction?

Hsp90 is a homodimeric ATPase and great progress has been made in understanding the ATPase driven conformational changes that Hsp90 can undergo [21,22]. Hsp90 contains three domains referred to as N-terminal (N), Middle (M), and C-terminal (C). The C domain forms a stable homodimer [23], while the N domain is the site of nucleotide binding and can form a transient dimer that is stimulated by ATP, but not ADP binding [24,25]. In full length Hsp90, dimerization of the N domain leads to a closed state while N-domain dissociation leads to an open state. Large structural transition between the open and closed states are caused primarily by hinge regions between the N, M, and C domains. In addition to the changes in the hinge regions, the other major ATP-driven conformation of Hsp90 is in the lid region of the N domain that closes over ATP, but not ADP or nucleotide-free structures [26]. How these ATPase driven conformational changes lead to client maturation remain unclear [27] and are a major focus of current research efforts.

We investigated dominant negative mutations to provide a new approach to study mechanism in Hsp90. Based on current knowledge of Hsp90, we anticipated three main categories of dominant negative Hsp90 mutations (Figure 1). Cross dimerization of a mutant subunit with WT Hsp90 may lead to a defective heterodimer for many reasons (e.g. loss of binding to critical client or co-chaperone), that we reasoned would be difficult to elucidate in detail. To minimize this dominant mechanism in our analyses, we used an engineering strategy that prevents WT from cross dimerizing with our mutant variants (further described in results and methods). Based on previous consideration of dominant negative mutations [4], we also anticipated that they may lead to tight binding to a critical partner protein making it inaccessible to WT Hsp90 (Figure 1B). Based on Hsp90's role with CHIP in triage decisions, we also speculated a new dominant mechanism where variants of Hsp90 stimulated the degradation of critical client proteins (Figure 1C).

**Results and Discussion**

To experimentally identify dominant negative Hsp90 mutations we drove expression of mutant variants from the Gal1 promoter (Figure 2). The Gal1 promoter (pGal1) is tightly regulated and so that there is no measurable expression when yeast are grown in dextrose, but strong expression is induced with galactose as the sugar source. With this approach, libraries of plasmid-encoded Hsp90 variants were transformed into yeast and the bulk culture expanded in dextrose media. Without expression of the mutant Hsp90, all variants could amplify independent of potential toxic effects of the encoded protein. Transfer of the bulk culture to galactose media then induced expression of the mutant Hsp90 variants along with WT Hsp90 whose expression was driven by a constitutive promoter whose strength was independent of the sugar source. This coordinated the initiation of co-expression selection in the bulk culture that we monitored by

deep sequencing before and after galactose induction. We included a small coiled-coil motif with WT Hsp90 that superstabilizes the dimer and virtually eliminates cross-dimerization with Hsp90 variants without the coiled-coil [28]. Our library of variants lacked the coiled-coil domain, so that the potential dominant effects of these mutants were assessed in an otherwise native background (Figure 2B).

We had previously performed a single-expression mutational scan of Hsp90 (REF) and noticed that some variants were unobserved. In the single-expression scan, the mutant library was driven by a constitutive promoter and WT Hsp90 from the Gal1 promoter (Figure 2A). Bulk cultures of variants were amplified in galactose media (co-expression conditions) before competition in dextrose media (single-expression conditions). While we suspected that variants that were unobserved or at very low frequency after amplification were toxic, we could not rule out the possibility that they did not get into yeast cells during transformation. In addition, WT in the single-expression scans did not contain a coiled-coil and so could readily cross-dimerize with mutant variants. Potential toxic effects in the single-expression experiments could be due to defective mutant/WT cross dimers.

We noted that the amino acids that were missing in our single expression screen were predominantly in the hinge regions that mediate the closing and opening of the lid that closes over ATP in the N domain of Hsp90 (Figure 3). We decided to focus our experimental analysis of dominant mutations on these regions. We generated a pGal1-driven systematic library of all possible point mutations across positions 92-101 and 122-131 that contains these hot spots of potential dominant variants, competed them in bulk competition, and quantified potential toxic effects based on frequency changes in deep sequencing readouts.

Internal controls indicate that our mutational scanning measurements were accurate. Silent mutations that do not change the amino acid sequence, do not exhibit dominant effects (squares with dots in Figure 3B). This finding indicates that selection in our experiments was predominantly on the protein sequence and not the DNA or RNA sequences that encode the protein. Stop codons also do not show any strong dominant growth effects (top row in Figure 3B), indicating that truncated protein products in these regions of Hsp90 are well tolerated when WT Hsp90 is co-expressed.

Within these hinge regions, we identified 140 amino acid substitutions that caused significant ($p<0.05$ based on Z-scores) dominant negative effects (Figure 3). This represents 37% (140/380) of all possible single amino acid changes. Of note, the toxic effects of so many amino acid changes in these regions may impose especially stringent selection pressure on translation accuracy. It will be interesting to examine if there is evidence of stringent selection for translation accuracy by comparing nucleotide sequence diversity in these regions compared to other regions in Hsp90.

There is large and significant ($p < 0.0001$ based on $Chi^2$ test) overlap between the set of dominant negative mutations we directly observed in the hinge regions and mutations that were missing in the single expression screen (Figure 3D). This observation indicates that missing amino

acids in the single expression screen were commonly due to dominant negative effects and not due to an inability of the plasmid-encoded variants to transform into cells. It also indicates that most dominant negative mutations have toxic effects independent of cross-dimerization with WT subunits because this cross-dimerization was limited in our co-expression experiments, but not our single-expression screen.

There was a broad range of dominant growth effects of mutations in the hinge regions (Figure 4). There was a narrow clustering of effects for both silent mutations and stop codons at different positions, indicating both the reproducibility of the experiments and that selection was predominantly acting on the protein sequence and not the nucleic acid sequence. We chose a conservative approach to categorize the strongest dominant negative substitutions with growth effects of less than -0.4, which represents four standard deviations less than the average stop codon. Of note, the toxic effects of stop codons are similar in magnitude to effects previously observed in yeast for the expression of folding compromised GFP [29]. Given the position of the hinge region in the middle of the primary sequence of the N domain, stop mutations likely result in misfolded proteins that act to slow growth.

Given the new approach for identifying dominant negative mutations in Hsp90, we sought multiple lines of evidence to confirm the results. We examined the reproducibility of dominant negative substitutions encoded by different synonymous mutations in the bulk competition (Figure 4B). Independent of the synonymous mutation encoding dominant negative mutations, we observed similar dominant growth effects, indicating that the measurements were strongly reproducible. We also cloned individual dominant negative variants and confirmed their toxic effects for yeast growth both on plates and in liquid culture (Figures 4C&D).

Motivated by the structural role of the hinge region in closing over bound ATP, we examined how ATP hydrolysis impacted the dominant effects of individual mutations. We chose to investigate the A97L, G123H and F124N dominant negative mutations because they showed strong reproducibility in the bulk competitions and exhibited some of the strongest growth defects. To block ATP hydrolysis, we added the E33A mutation. In WT Hsp90, E33 positions a water molecule for ATP hydrolysis [24]. Previous studies have shown that the E33A mutation is compatible with ATP binding but prevents hydrolysis [30]. In the context of all three different dominant negative mutations we analyzed, E33A dramatically reduced toxic effects on growth (Figure 5A). This result indicates that these mutations exert their toxic effects through a dynamic ATPase driven mechanism. Of note, pull down experiments of dominant negative variants from Hsp90 did not reveal any strong binding partners (data not shown), consistent with dynamic conformations and complexes leading to the observed toxicity.

We further interrogated the role of ATPase activity on the biochemical properties of the F124N Hsp90 variant in purified form. F124N showed moderately elevated basal ATPase activity in vitro (Figure 5B). The ATPase activity of F124N responded to co-chaperones similarly to WT Hsp90 – stimulated by Aha1 and Hch1 and retarded by Sba1. Previous studies have demonstrated that a wide range of at least two orders of magnitude of basal ATPase activity is compatible with robust yeast growth [31]. In purified form, the ATPase activity of F124N is within a range that is

compatible with robust yeast growth and it responds to co-chaperones similarly to WT Hsp90. The toxic properties of F124N do not appear to be due to gross disturbance of ATPase activity, or co-chaperone interactions.

ATP binding induces a large open to closed conformational change in WT Hsp90 [25], and we examined how the F124N mutation impacted ATP-driven structural rearrangements (Figure 5C). We used a FRET approach originally developed by Buchner and colleagues [32] to monitor the conformation of purified full-length Hsp90 in the presence and absence of the ATP analogue ATPγS. Similar to previous observations, the ATP analogue stimulates a closed state for WT Hsp90. However, the FRET signal in the presence of ATPγS is greatly reduced for F124N compared to WT Hsp90, suggesting that F124N is not able to readily form a closed structure. Multiple studies including single molecule fluorescent analyses, indicate that the formation of a closed ATP bound structure is a consistent part of the ATPase driven conformational cycle of Hsp90 [33]. Our findings with F124N indicate that ATPase activity does not require forming a closed conformation, but when the linkage between ATPase activity and formation of the closed structure is disrupted, it causes critical challenges for cell growth.

Motivated by the role of Hsp90 in triage decisions targeting clients for degradation in mammalian systems [17,19] and the dynamic ATPase properties of F124N, we investigated client stability to proteolysis (Figure 6). Induction of two different dominant negative Hsp90 variants (F124N and G123H) both led to large decreases in the levels of the model client protein GR. These results demonstrate that dominant negative Hsp90 variants can lead to a decrease in the accumulation of a client protein.

Based on all our observations, we propose a model where formation of an ATP-bound closed Hsp90 structure is important for promoting the maturation of client proteins and dominant negative mutations destabilize clients by hydrolyzing ATP from a more open structure (Figure 7). This model is consistent with dominant negative mutant effects depending on ATP hydrolysis, failing to form a closed structure, and promoting the destruction of a client protein.

**Conclusions**

Our findings provide strong evidence for an evolutionarily conserved function of Hsp90 in triage decisions for client proteins and provides insights into its mechanism. Prior studies had shown that the mammalian-specific Hsp90 co-chaperone CHIP can help to mediate triage decisions by Hsp90 [18]. Multiple studies have also shown that competitive ATP inhibitors of Hsp90 lead to the ubiquitin targeted degradation of many clients in mammalian cells [17,20]. It has also been shown that many mammalian E3's physically bind to Hsp90 [10], though it was unclear if this indicated that they were clients or acting to assist in triage decisions. Our work demonstrates that Hsp90 can target clients for degradation in yeast and that this is property is enhanced in dominant mutations that hydrolyze ATP without forming a fully closed state. This mechanism has a number of important potential implications that will be interesting to investigate in future studies. For example, we speculate that this mechanism of targeting clients for degradation may occur infrequently in the ATPase cycle of WT Hsp90 such that clients that stay bound through multiple

cycles will eventually be targeted for degradation. In addition, this mechanism may be at play in the action of Hsp90 while bound to competitive ATP inhibitors. Our study demonstrates that triage decisions are an inherent and evolutionarily conserved property of Hsp90 and that hydrolysis of ATP in the closed state of Hsp90 is critical for keeping clients on the maturation pathway as opposed to the degradation pathway.

This work also demonstrates that dominant negative mutations can provide powerful new views of biologically important mechanism, especially for highly dynamic protein hubs such as Hsp90. This is one of the most important, but poorly understood areas of protein science. Systematic identification of dominant negative mutations can be widely utilized to study the mechanism of other important genes.

## Material and Methods

*Library construction*

Point mutation libraries were generated in p417 plasmids using a cassette ligation strategy as previously described [34]. To construct the libraries for the co-expression experiment, a destination vector was generated using a pRS414 plasmid containing the GalS promoter [35] and the first and last 30 bases of Hsp90 bracketing a SphI restriction site. Two 10 consecutive amino acid saturation mutagenesis libraries covering amino acids 92-101 and 122-131 of Hsp90 were excised from the p417 plasmids using restriction enzymes that cut immediately upstream and downstream of the Hsp90 gene and annealed into the destination vector cut with SphI using SLIC cloning as described [36,37]. The number of independent transformants was in large excess to the library diversity.

*Strain construction*

To avoid forming heterodimers between the mutant and wild-type versions of Hsp90, a strain was created in which a coiled-coil version of Hsp90 was the sole Hsp90 expressed in the yeast strain. To do this, we used the haploid Saccharomyces cerevisiae ECU82a plasmid swap strain, which is a derivative of W303 in which both endogenous Hsp90 genes, hsp82 and hsc82 are knocked out and wild-type hsp82 gene is expressed from a pKAT6 URA3 marked plasmid amenable to negative selection [38]. The Hsp90-coil construct containing a coiled-coil sequence (GGGTSSVKELEDKNEELLSEIAHLKNEVARLKKLVGERTG) inserted after amino acid 678 of Hsp90 [28] driven by a constitutive GPD promoter together with a HIS3 marker was integrated into the HO genomic locus of the plasmid swap strain. The resulting transformants were grown on plates containing 5-fluoroorotic acid, which selects for loss of the pKAT6 plasmid, to create the strain JFY12 (can1-100 ade2-1 his3-11,15 leu2-3,12 trp1-1 ura3-1 hsp82::leu2 hsc82::leu2 ho::pgpd-hsp82-coil-his3).

*Bulk competition experiment (co-expression)*

The JFY12 strain was transformed with the two p414Gal Hsp90 libraries (aa 91-101 and aa 121-131) using the lithium acetate method at a transformation efficiency sufficient to obtain a greater than 50-fold coverage of each mutant in each library (100,000 total transformants). Following 12 hours of recovery in synthetic dextrose lacking histidine (SD-H), transformed cells

were washed three times in synthetic dextrose lacking histidine and tryptophan (SD-H-W to select for the presence of the Hsp90 library plasmid) to remove extracellular DNA, and grown in 50 mL SD-H-W media at 30°C for 24 hours with repeated dilutions to maintain the cells in log phase of growth and to expand the library. At least $10^7$ cells were passed for each dilution to avoid population bottlenecks. Cells in log growth were washed twice in synthetic 2% raffinose media lacking histidine and tryptophan (SRaf-H-W), diluted to early log phase in 50 mL SRaf-H-W and grown for 16 hours until the cultures reached mid-log phase. To begin the bulk competition experiment, cells were diluted to early log phase in synthetic 1% raffinose, 1% galactose media lacking tryptophan and histidine (SRafGal-H-W). An initial 0 hour time point was collected of ~$10^8$ cells, pelleted, washed, and stored at -80C. The remaining cells were grown for 30 hours at 30°C with samples collected as before at various time points (5, 8,11,14,17,25,28 and 30 hours).

*Bulk competition experiment (single-expression)*

For the single-expression competition experiment, point mutation libraries covering amino acids 12-231 were transferred as above to a p414GPD destination vector, which constitutively expresses Hsp90 at endogenous yeast levels [38]. The libraries were transferred in 10 amino acid segments to ensure complete coverage of the library. The p414GPD Hsp90 libraries were then transformed into the DBY288 Hsp90 shutoff strain (can1-100 ade2-1 his3-11,15 leu2-3,12 trp1-1 ura3-1 hsp82::leu2 hsc82::leu2 ho::pgals-hsp82-his3) [39] which was generated from the Ecu Hsp90 plasmid swap strain [38] by integration of Hsp90 driven by a Gal promoter [35] together with a HIS3 marker into the HO genomic locus. Bulk competition experiments were performed as described [40]. In short, mutant libraries were amplified in the presence of wild-type Hsp90 in SRafGal-H-W, and then switched to wild-type shutoff conditions in SD-H-W media for 16 hours at 30°C. A sample of the culture was pelleted and stored at -80°C at this point and after a further 8 hours of competition. Libraries containing 10 consecutive amino acids were competed and analyzed in separate cultures in order to facilitate efficient analyses of mutant frequency using focused next-generation sequencing. All mutants were analyzed in parallel in the same batch of media with competition cultures grown on the same day in the same incubator. Cultures were maintained in log phase by regular dilution with fresh media and managed to maintain a population size of $10^9$ or greater to minimize impacts from bottlenecking. Sample processing for next-generation sequencing and data analyses were performed as previously described [34].

*Yeast growth analysis*

To determine the growth rate of individually cloned Hsp90 mutants, a panel of Hsp90 point mutations were individually cloned by site-directed mutagenesis into the p414Gal vector and transformed into JFY12 using a lithium-acetate based procedure. Individual clones were selected on SD-H-W media where expression of the mutants was not induced. Clones were grown in liquid SD-H-W media to a cell density of $10^8$ at 30°C, washed with SRaf-W-H to remove residual dextrose and diluted to early log growth phase in SRaf-H-W and grown for 16 hours at 30°C. Cells were then diluted to early log phase in SRafGal-H-W to induce the expression of the mutants. The growth rate of the cultures was monitored based on absorbance at 600 nm over time and fit to an exponential growth model [37]. During this time, the cells were maintained in

log phase by periodic dilution. Additionally, after 8 hours of growth in the SRafGal-H-W induction media, spotting assays were performed. Serial 10-fold dilutions of each culture was spotted on both SRafGal-W-H (to induce mutant Hsp90 expression) and SD-H-W (control – no mutant expression) and incubated for 2 days at 30°C to monitor colony growth.

*Analysis of steady state levels of GR*

To determine the impact of the DN Hsp90 variants on the steady state levels of GR, the JFY12 strain was transformed with p414Gal plasmids expressing either WT, F124N or G123H Hsp90 and the P2A/GRGZ plasmid described previously that constitutively expresses GR [41]. Cells were grown as above and harvested after 6 hours of growth in inductive media (SRafGal-W-A). Frozen yeast pellets were thawed on ice and lysed using glass beads in a lysis buffer containing 5mM EDTA, 50mM tris pH 8, and both 5mM PMSF and protease inhibitor cocktail as protease inhibitors. The total protein concentration in each lysate was estimated using a BCA assay. The lysate was analyzed via SDS-PAGE electrophoresis and western blotting. The PVDF membrane was blocked in 5% milk and TBS (tris buffered saline) at room temperature for 1 hour. After blocking, the membrane was probed with the FLAG (FG4R) primary antibody at a 1:5000 dilution in 1% milk and TBS overnight at 4°C. After washing in 1xTBS, the membrane was incubated in anti-mouse secondary conjugated to HRP at a 1:5000 dilution in 4% milk and TBS for 1 hour at room temperature. The surface of the membrane was incubated in ECL substrate for 5 minutes. Bands were visualized using chemiluminescence.

*Purification of Hsp90*

Hsp90 variants with N-terminal $His_6$ tags were bacterially expressed, purified and analyzed as described previously [23]. In brief, protein purification was performed using Co+NTA agarose (Qiagen), followed by a Phenyl Sepharose column, and a Q sepharose HP column (GE). Aha1 and Hch1 were purified as previously described [41,42]. The concentrations of these highly purified proteins were determined spectroscopically using extinction coefficients based on amino acid composition.

*ATPase assay*

Hydrolysis of ATP by Hsp90 was determined using an NADH-coupled ATPase assay as previously described [43]. ATPase assays were performed at 37C in 20 mM Tris pH 7.5, 5 mM MgCl2, 100 mM KCl using a Bio50 Spectrophotometer equipped with a Peltier temperature control unit (Cary) and a 1 cm pathlength cuvette. The reaction was initiated by the addition of 2 mM ATP. Absorbance at 340 nm ($\varepsilon 340 = 6220\ M^{-1}\ cm^{-1}$) was measured at 15 second intervals for 10 min as previously described [23].

*FRET labeling and assay*

Hsp90 was labeled with donor and acceptor dyes (ATTO-488- maleimide and ATT0-550-maleimide) (company) as recommended by the manufacturer at an engineered cysteine residue (D61C) [32]. 2 µM donor-labeled and 2 µM acceptor labeled Hsp90 were mixed in 20 mM Tris pH 7.5, 5 mM $MgCl_2$, 100 mM KCl and incubated at 37°C for 30 minutes to allow subunit exchange followed by addition of the indicated concentration of ATPγS and FRET was measured in a Fluoromax 3 machine at 37°C.

**Acknowledgements**

This works was supported by grant R01-GM112844 from the National Institutes of Health to D.N.A.B.

**Figure Legends**

**Figure 1. Potential dominant negative mechanisms for Hsp90.** (A) Formation of inactive heterodimers with WT subunits. (B) Tight binding to critical binding partners that sequesters them from interacting with WT Hsp90. (C) Stimulation of the degradation of essential proteins.

**Figure 2. Comparison of screens for loss of function and dominant negative Hsp90 variants.** The top panel shows a previously published screen for loss of function Hsp90 variants where selection occurs with mutant variants in the absence of WT expression . The bottom panel shows the screen for dominant negative mutants where selection occurs with WT co-expressed.

**Figure 3. Identification of dominant negative Hsp90 variants.** (A) Identification of hot-spots for potential dominant negative mutations based on variants that were missing in the previously published single expression screen [44]. The plot shows positions in the N domain which was where the majority of missing mutations were identified. (B) Heatmap representation of dominant effects from a co-expression screen of all point mutations in the lid hinge regions. (C) Molecular representation of the N domain highlighting the location of the lid hinge regions. (D) Overlap of mutations identified as dominant negative in the co-expression screen with those missing in the single-expression screen. The overlap is significant ($p<0.00001$, $chi^2$).

**Figure 4. Reproducibility and validation of dominant negative variants.** (A) Distribution of growth effects. Variants with growth effects lower than -0.4 were classified as dominant negative. (B) Variation in growth effects among synonymous codons for the same amino acid substitution. (C&D) Growth properties of individually isolated dominant negative variants on plates (C) and in liquid culture (D).

**Figure 5. Impacts of dominant negative mutations on ATP-driven conformational changes.** (A) The E33A mutation that prevents ATP hydrolysis in Hsp90 rescues the toxic effects of multiple dominant negative mutations. (B) ATPase rate of purified Hsp90 in the presence and absence of co-chaperones. (C) Conformation of fluorescently labeled WT and F124N Hsp90 protein monitored by FRET.

**Figure 6. Dominant negative Hsp90 destabilizes a model client to degradation.**

**Figure 7. Model of the mechanism of dominant negative Hsp90 variants.**

**References**

(1) Stiller, J. B.; Otten, R.; Häussinger, D.; Rieder, P. S.; Theobald, D. L.; Kern, D. Structure Determination of High-Energy States in a Dynamic Protein Ensemble. *Nature* **2022**, *603* (7901), 528–535. https://doi.org/10.1038/s41586-022-04468-9.

(2) Noji, H.; Yasuda, R.; Yoshida, M.; Kinosita, K. Direct Observation of the Rotation of F1-ATPase. *Nature* **1997**, *386* (6622), 299–302. https://doi.org/10.1038/386299a0.

(3) Heller, A.; Feldman, B. Electrochemical Glucose Sensors and Their Applications in Diabetes Management. *Chem Rev* **2008**, *108* (7), 2482–2505. https://doi.org/10.1021/cr068069y.

(4) Herskowitz, I. Functional Inactivation of Genes by Dominant Negative Mutations. *Nature* **1987**, *329* (6136), 219–222. https://doi.org/10.1038/329219a0.

(5) Miller, R. T.; Masters, S. B.; Sullivan, K. A.; Beiderman, B.; Bourne, H. R. A Mutation That Prevents GTP-Dependent Activation of the Alpha Chain of Gs. *Nature* **1988**, *334* (6184), 712–715. https://doi.org/10.1038/334712a0.

(6) Mathy, C. J. P.; Mishra, P.; Flynn, J. M.; Perica, T.; Mavor, D.; Bolon, D. N. A.; Kortemme, T. A Complete Allosteric Map of a GTPase Switch in Its Native Cellular Network. *Cell Syst* **2023**, *14* (3), 237-246.e7. https://doi.org/10.1016/j.cels.2023.01.003.

(7) Padhy, A. A.; Mavor, D.; Sahoo, S.; Bolon, D. N. A.; Mishra, P. Systematic Profiling of Dominant Ubiquitin Variants Reveals Key Functional Nodes Contributing to Evolutionary Selection. *Cell Rep* **2023**, *42* (9), 113064. https://doi.org/10.1016/j.celrep.2023.113064.

(8) Borkovich, K. A.; Farrelly, F. W.; Finkelstein, D. B.; Taulien, J.; Lindquist, S. Hsp82 Is an Essential Protein That Is Required in Higher Concentrations for Growth of Cells at Higher Temperatures. *Mol Cell Biol* **1989**, *9* (9), 3919–3930. https://doi.org/10.1128/mcb.9.9.3919-3930.1989.

(9) Schopf, F. H.; Biebl, M. M.; Buchner, J. The HSP90 Chaperone Machinery. *Nat Rev Mol Cell Biol* **2017**, *18* (6), 345–360. https://doi.org/10.1038/nrm.2017.20.

(10) Taipale, M.; Krykbaeva, I.; Koeva, M.; Kayatekin, C.; Westover, K. D.; Karras, G. I.; Lindquist, S. Quantitative Analysis of HSP90-Client Interactions Reveals Principles of Substrate Recognition. *Cell* **2012**, *150* (5), 987–1001. https://doi.org/10.1016/j.cell.2012.06.047.

(11) Smith, D. F.; Toft, D. O. Minireview: The Intersection of Steroid Receptors with Molecular Chaperones: Observations and Questions. *Mol Endocrinol* **2008**, *22* (10), 2229–2240. https://doi.org/10.1210/me.2008-0089.

(12) Picard, D.; Khursheed, B.; Garabedian, M. J.; Fortin, M. G.; Lindquist, S.; Yamamoto, K. R. Reduced Levels of Hsp90 Compromise Steroid Receptor Action in Vivo. *Nature* **1990**, *348* (6297), 166–168. https://doi.org/10.1038/348166a0.

(13) Wang, R. Y.-R.; Noddings, C. M.; Kirschke, E.; Myasnikov, A. G.; Johnson, J. L.; Agard, D. A. Structure of Hsp90-Hsp70-Hop-GR Reveals the Hsp90 Client-Loading Mechanism. *Nature* **2022**, *601* (7893), 460–464. https://doi.org/10.1038/s41586-021-04252-1.

(14) Neckers, L.; Workman, P. Hsp90 Molecular Chaperone Inhibitors: Are We There Yet? *Clin Cancer Res* **2012**, *18* (1), 64–76. https://doi.org/10.1158/1078-0432.CCR-11-1000.

(15) Whitesell, L.; Mimnaugh, E. G.; De Costa, B.; Myers, C. E.; Neckers, L. M. Inhibition of Heat Shock Protein HSP90-Pp60v-Src Heteroprotein Complex Formation by Benzoquinone Ansamycins: Essential Role for Stress Proteins in Oncogenic Transformation. *Proc Natl Acad Sci U S A* **1994**, *91* (18), 8324–8328. https://doi.org/10.1073/pnas.91.18.8324.

(16) Jaeger, A. M.; Whitesell, L. HSP90: Enabler of Cancer Adaptation. *Annu. Rev. Cancer Biol.* **2019**, *3* (1), 275–297. https://doi.org/10.1146/annurev-cancerbio-030518-055533.

(17) An, W. G.; Schulte, T. W.; Neckers, L. M. The Heat Shock Protein 90 Antagonist Geldanamycin Alters Chaperone Association with P210bcr-Abl and v-Src Proteins before Their Degradation by the Proteasome. *Cell Growth Differ* **2000**, *11* (7), 355–360.

(18) Kundrat, L.; Regan, L. Balance between Folding and Degradation for Hsp90-Dependent Client Proteins: A Key Role for CHIP. *Biochemistry* **2010**, *49* (35), 7428–7438. https://doi.org/10.1021/bi100386w.

(19) Quintana-Gallardo, L.; Martín-Benito, J.; Marcilla, M.; Espadas, G.; Sabidó, E.; Valpuesta, J. M. The Cochaperone CHIP Marks Hsp70- and Hsp90-Bound Substrates for Degradation through a Very Flexible Mechanism. *Sci Rep* **2019**, *9* (1), 5102. https://doi.org/10.1038/s41598-019-41060-0.

(20) Faresse, N.; Ruffieux-Daidie, D.; Salamin, M.; Gomez-Sanchez, C. E.; Staub, O. Mineralocorticoid Receptor Degradation Is Promoted by Hsp90 Inhibition and the Ubiquitin-Protein Ligase CHIP. *American Journal of Physiology-Renal Physiology* **2010**, *299* (6), F1462–F1472. https://doi.org/10.1152/ajprenal.00285.2010.

(21) Richter, K.; Soroka, J.; Skalniak, L.; Leskovar, A.; Hessling, M.; Reinstein, J.; Buchner, J. Conserved Conformational Changes in the ATPase Cycle of Human Hsp90. *Journal of Biological Chemistry* **2008**, *283* (26), 17757–17765. https://doi.org/10.1074/jbc.M800540200.

(22) Mickler, M.; Hessling, M.; Ratzke, C.; Buchner, J.; Hugel, T. The Large Conformational Changes of Hsp90 Are Only Weakly Coupled to ATP Hydrolysis. *Nat Struct Mol Biol* **2009**, *16* (3), 281–286. https://doi.org/10.1038/nsmb.1557.

(23) Wayne, N.; Bolon, D. N. Dimerization of Hsp90 Is Required for in Vivo Function. Design and Analysis of Monomers and Dimers. *J Biol Chem* **2007**, *282* (48), 35386–35395. https://doi.org/10.1074/jbc.M703844200.

(24) Ali, M. M. U.; Roe, S. M.; Vaughan, C. K.; Meyer, P.; Panaretou, B.; Piper, P. W.; Prodromou, C.; Pearl, L. H. Crystal Structure of an Hsp90-Nucleotide-P23/Sba1 Closed Chaperone Complex. *Nature* **2006**, *440* (7087), 1013–1017. https://doi.org/10.1038/nature04716.

(25) Southworth, D. R.; Agard, D. A. Species-Dependent Ensembles of Conserved Conformational States Define the Hsp90 Chaperone ATPase Cycle. *Molecular Cell* **2008**, *32* (5), 631–640. https://doi.org/10.1016/j.molcel.2008.10.024.

(26) Prodromou, C.; Roe, S. M.; O'Brien, R.; Ladbury, J. E.; Piper, P. W.; Pearl, L. H. Identification and Structural Characterization of the ATP/ADP-Binding Site in the Hsp90 Molecular Chaperone. *Cell* **1997**, *90* (1), 65–75. https://doi.org/10.1016/S0092-8674(00)80314-1.

(27) Pullen, L.; Bolon, D. N. Enforced N-Domain Proximity Stimulates Hsp90 ATPase Activity and Is Compatible with Function in Vivo. *J Biol Chem* **2011**, *286* (13), 11091–11098. https://doi.org/10.1074/jbc.M111.223131.

(28) Wayne, N.; Lai, Y.; Pullen, L.; Bolon, D. N. Modular Control of Cross-Oligomerization: Analysis of Superstabilized Hsp90 Homodimers in Vivo. *J Biol Chem* **2010**, *285* (1), 234–241. https://doi.org/10.1074/jbc.M109.060129.

(29) Geiler-Samerotte, K. A.; Dion, M. F.; Budnik, B. A.; Wang, S. M.; Hartl, D. L.; Drummond, D. A. Misfolded Proteins Impose a Dosage-Dependent Fitness Cost and Trigger a Cytosolic Unfolded Protein Response in Yeast. *Proc. Natl. Acad. Sci. U.S.A.* **2011**, *108* (2), 680–685. https://doi.org/10.1073/pnas.1017570108.

(30) Panaretou, B.; Prodromou, C.; Roe, S. M.; O'Brien, R.; Ladbury, J. E.; Piper, P. W.; Pearl, L. H. ATP Binding and Hydrolysis Are Essential to the Function of the Hsp90 Molecular Chaperone in Vivo. *EMBO J* **1998**, *17* (16), 4829–4836. https://doi.org/10.1093/emboj/17.16.4829.

(31) Prodromou, C.; Panaretou, B.; Chohan, S.; Siligardi, G.; O'Brien, R.; Ladbury, J. E.; Roe, S. M.; Piper, P. W.; Pearl, L. H. The ATPase Cycle of Hsp90 Drives a Molecular "clamp" via Transient Dimerization of the N-Terminal Domains. *EMBO J* **2000**, *19* (16), 4383–4392. https://doi.org/10.1093/emboj/19.16.4383.

(32) Hessling, M.; Richter, K.; Buchner, J. Dissection of the ATP-Induced Conformational Cycle of the Molecular Chaperone Hsp90. *Nat Struct Mol Biol* **2009**, *16* (3), 287–293. https://doi.org/10.1038/nsmb.1565.

(33) Ratzke, C.; Berkemeier, F.; Hugel, T. Heat Shock Protein 90's Mechanochemical Cycle Is Dominated by Thermal Fluctuations. *Proc Natl Acad Sci U S A* **2012**, *109* (1), 161–166. https://doi.org/10.1073/pnas.1107930108.

(34) Hietpas, R.; Roscoe, B.; Jiang, L.; Bolon, D. N. A. Fitness Analyses of All Possible Point Mutations for Regions of Genes in Yeast. *Nat Protoc* **2012**, *7* (7), 1382–1396. https://doi.org/10.1038/nprot.2012.069.

(35) Mumberg, D.; Müller, R.; Funk, M. Regulatable Promoters of Saccharomyces Cerevisiae: Comparison of Transcriptional Activity and Their Use for Heterologous Expression. *Nucleic Acids Res* **1994**, *22* (25), 5767–5768. https://doi.org/10.1093/nar/22.25.5767.

(36) Li, M. Z.; Elledge, S. J. Harnessing Homologous Recombination in Vitro to Generate Recombinant DNA via SLIC. *Nat Methods* **2007**, *4* (3), 251–256. https://doi.org/10.1038/nmeth1010.

(37) Jiang, L.; Mishra, P.; Hietpas, R. T.; Zeldovich, K. B.; Bolon, D. N. A. Latent Effects of Hsp90 Mutants Revealed at Reduced Expression Levels. *PLoS Genet* **2013**, *9* (6), e1003600. https://doi.org/10.1371/journal.pgen.1003600.

(38) Nathan, D. F.; Lindquist, S. Mutational Analysis of Hsp90 Function: Interactions with a Steroid Receptor and a Protein Kinase. *Mol Cell Biol* **1995**, *15* (7), 3917–3925. https://doi.org/10.1128/MCB.15.7.3917.

(39) Hietpas, R. T.; Bank, C.; Jensen, J. D.; Bolon, D. N. A. Shifting Fitness Landscapes in Response to Altered Environments. *Evolution* **2013**, *67* (12), 3512–3522. https://doi.org/10.1111/evo.12207.

(40) Mishra, P.; Flynn, J. M.; Starr, T. N.; Bolon, D. N. A. Systematic Mutant Analyses Elucidate General and Client-Specific Aspects of Hsp90 Function. *Cell Rep* **2016**, *15* (3), 588–598. https://doi.org/10.1016/j.celrep.2016.03.046.

(41) Meyer, P.; Prodromou, C.; Liao, C.; Hu, B.; Mark Roe, S.; Vaughan, C. K.; Vlasic, I.; Panaretou, B.; Piper, P. W.; Pearl, L. H. Structural Basis for Recruitment of the ATPase Activator Aha1 to the Hsp90 Chaperone Machinery. *EMBO J* **2004**, *23* (3), 511–519. https://doi.org/10.1038/sj.emboj.7600060.

(42) Horvat, N. K.; Armstrong, H.; Lee, B. L.; Mercier, R.; Wolmarans, A.; Knowles, J.; Spyracopoulos, L.; LaPointe, P. A Mutation in the Catalytic Loop of Hsp90 Specifically Impairs ATPase Stimulation by Aha1p, but Not Hch1p. *J Mol Biol* **2014**, *426* (12), 2379–2392. https://doi.org/10.1016/j.jmb.2014.04.002.

(43) Nørby, J. G. Coupled Assay of Na+,K+-ATPase Activity. *Methods Enzymol* **1988**, *156*, 116–119. https://doi.org/10.1016/0076-6879(88)56014-7.

(44) Flynn, J. M.; Rossouw, A.; Cote-Hammarlof, P.; Fragata, I.; Mavor, D.; Hollins, C.; Bank, C.; Bolon, D. N. Comprehensive Fitness Maps of Hsp90 Show Widespread Environmental Dependence. *eLife* **2020**, *9*, e53810. https://doi.org/10.7554/eLife.53810.

Figure 1.

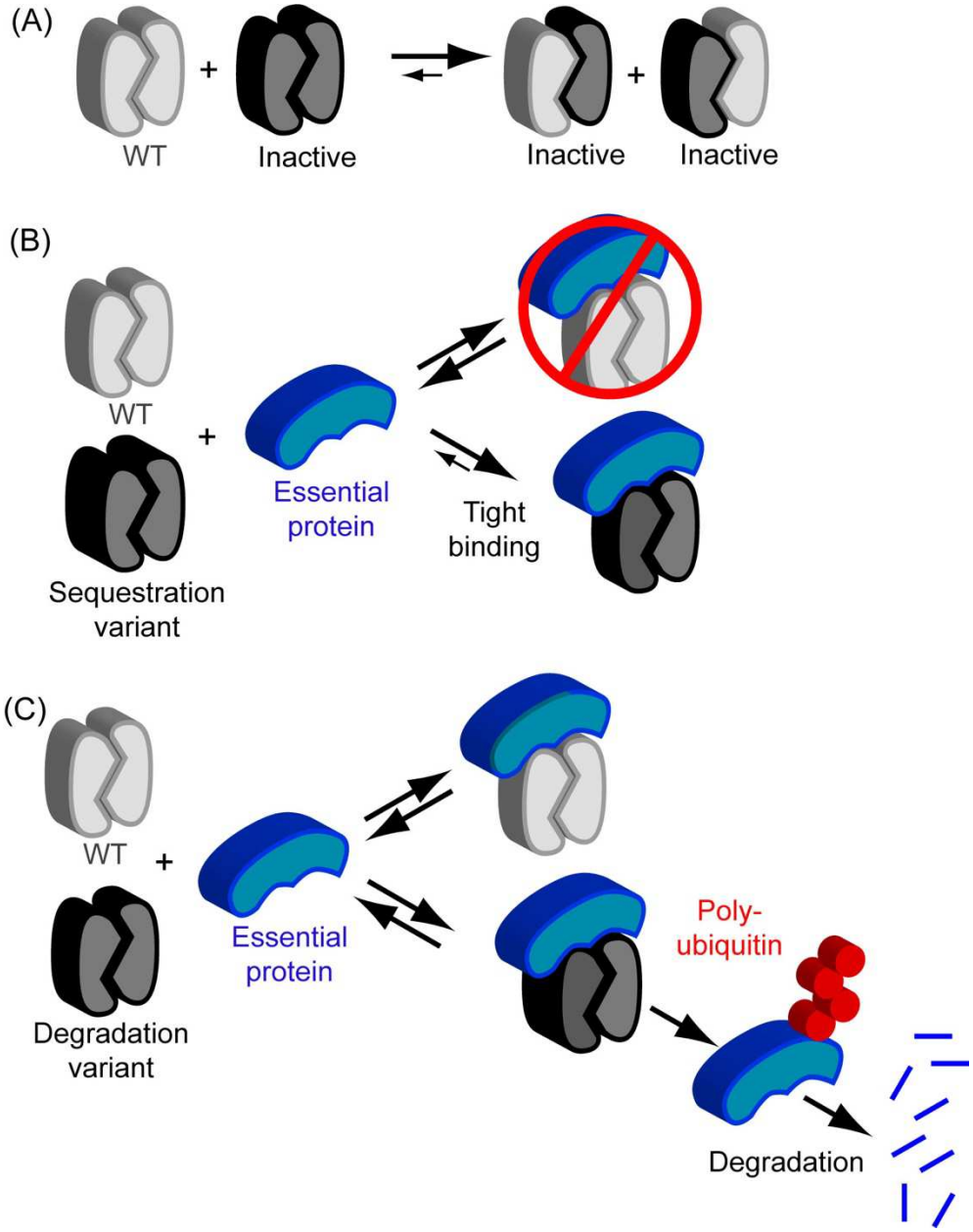

Figure 2

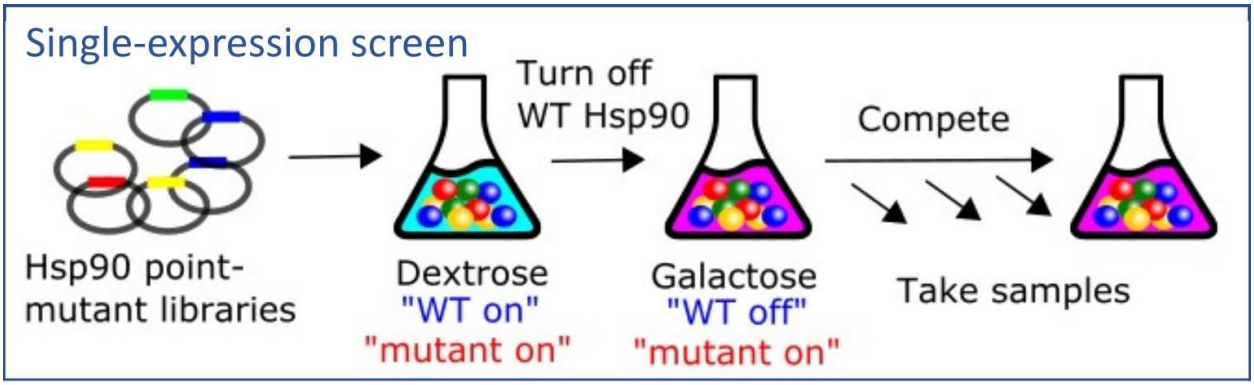


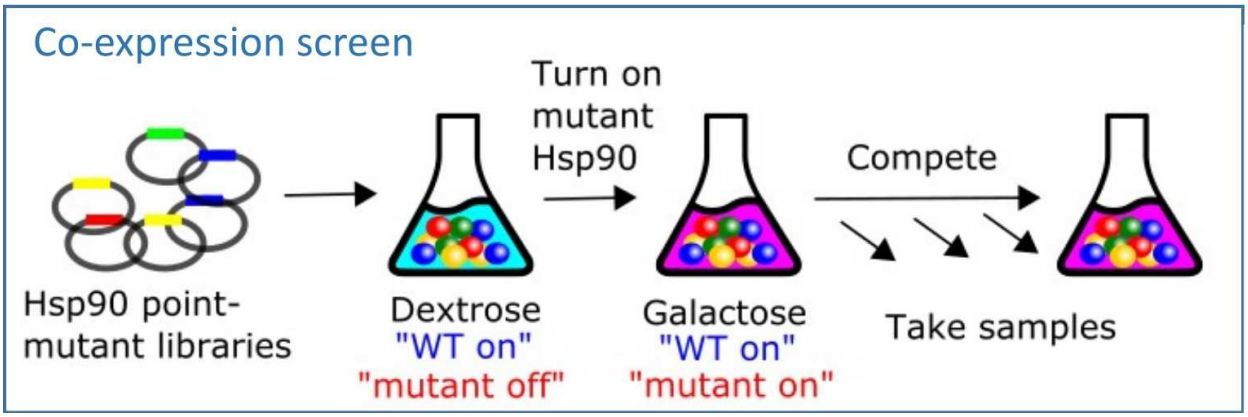

Figure 3

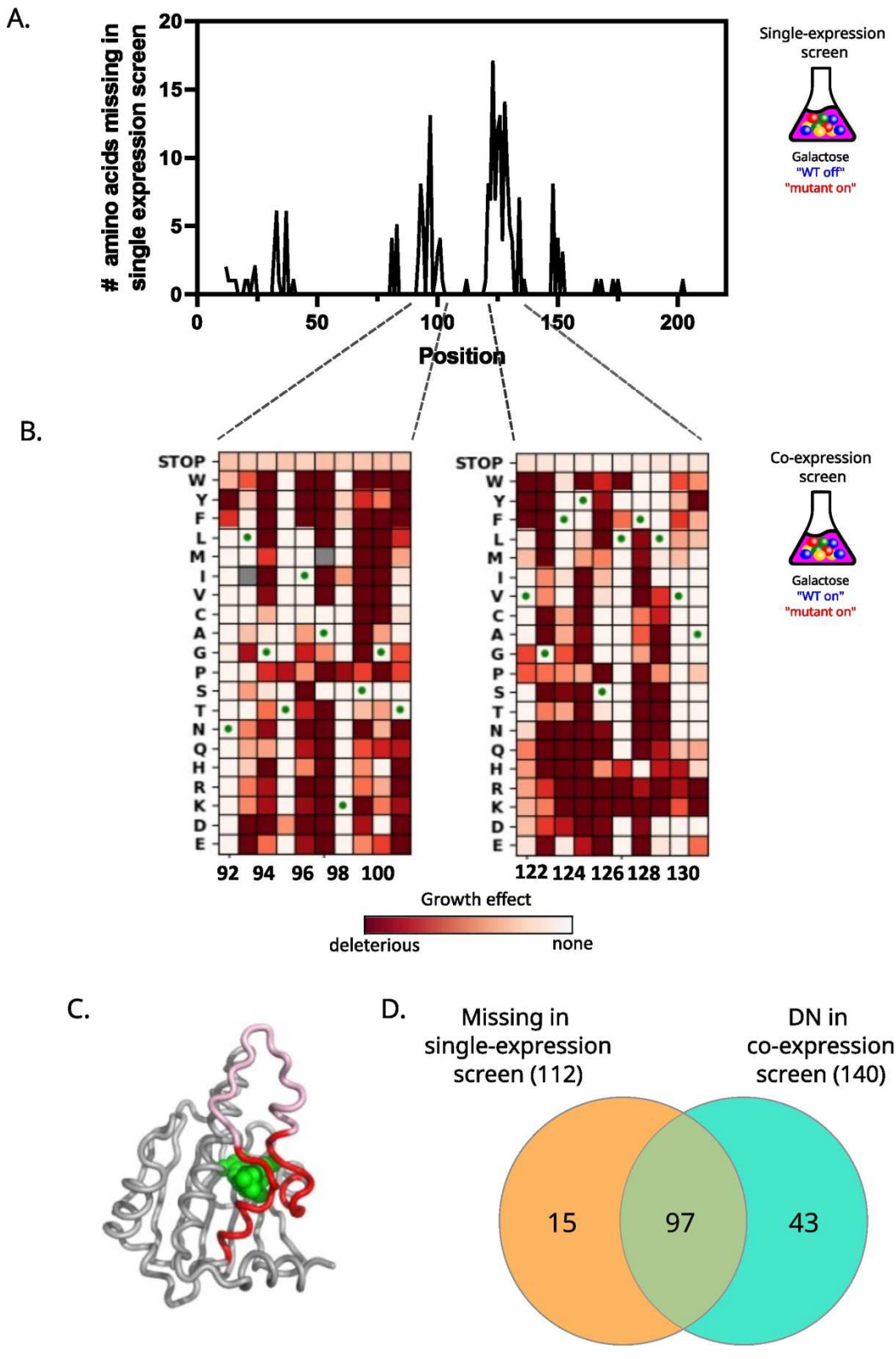

Figure 4

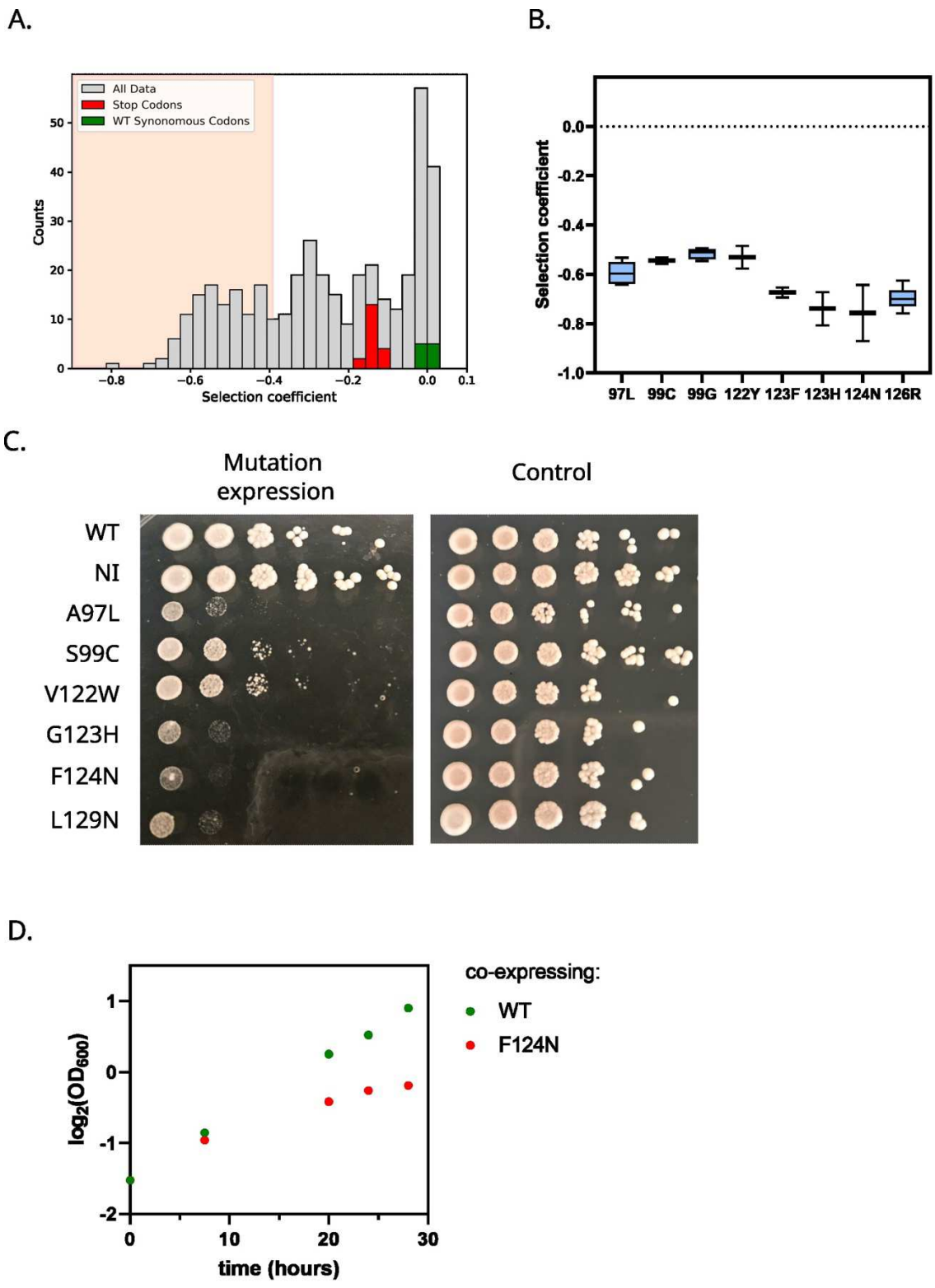

Figure 5

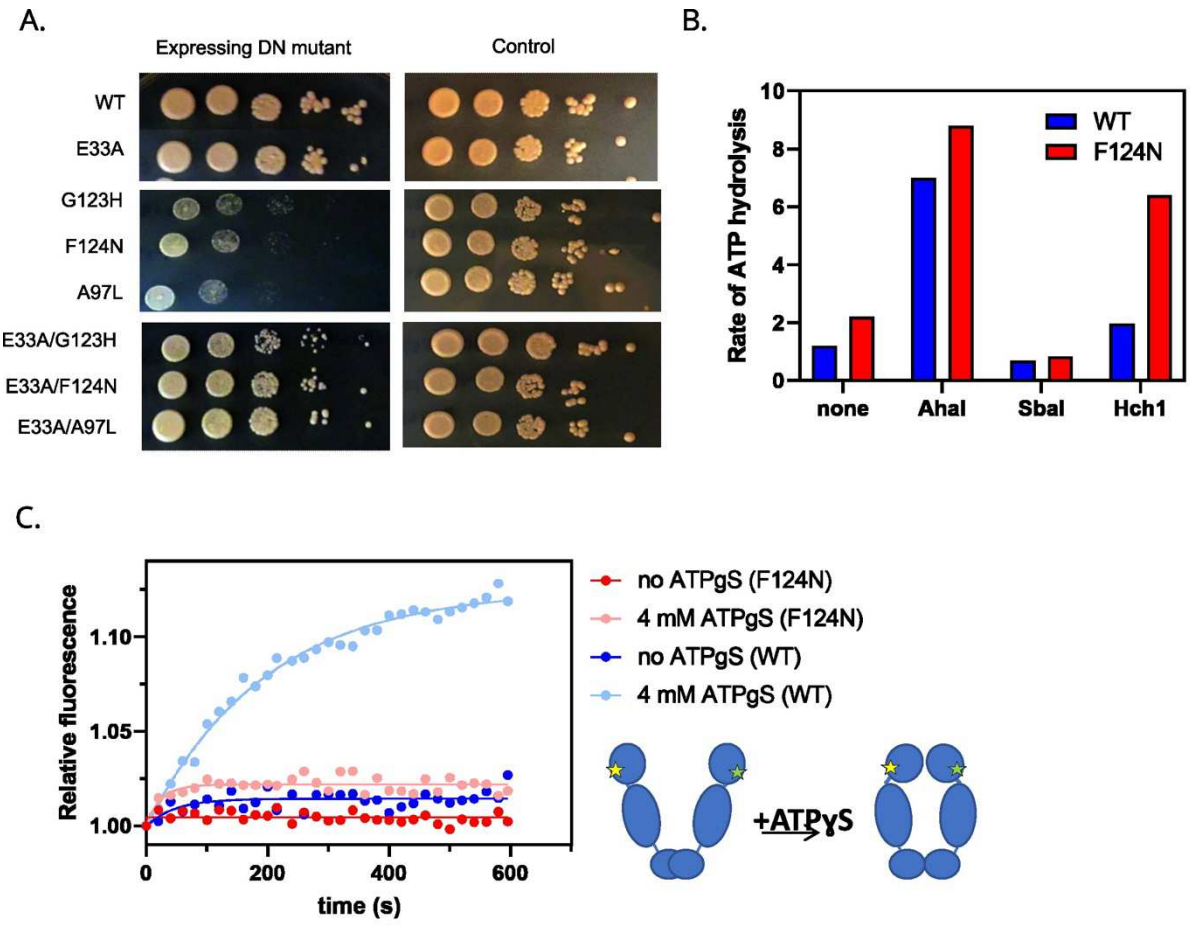

Figure 6

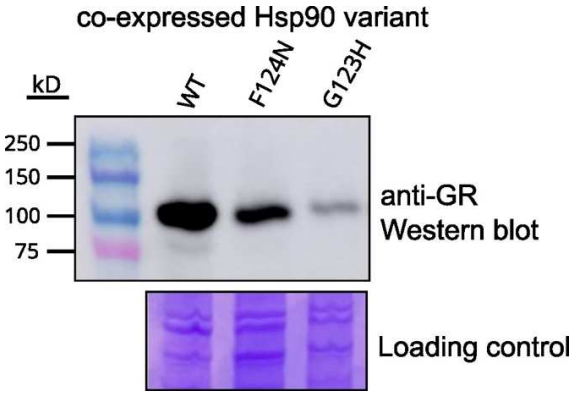

Figure 7.